Applied Acoustics 231 (2025) 110529

Contents lists available at ScienceDirect

Applied Acoustics

journal homepage: www.elsevier.com/locate/apacoust

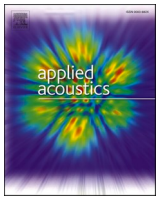

Experimental analysis of metamaterial with improved high sound levels absorption using complex frequency plane

Gauthier Bezançon [a,*], Olivier Doutres [a], Olga Umnova [b], Philippe Leclaire [c], Thomas Dupont [a]

[a] Department of Mechanical Engineering, École de Technologie Supérieure Montréal Québec Canada
[b] University of Salford Manchester England UK
[c] DRIVE – ISAT Université de Bourgogne Nevers France

ARTICLE INFO

Keywords:
Sound absorbers
Acoustic metamaterial
Multi-resonant material
High sound levels
Nonlinear regime
Complex frequency plane

ABSTRACT

This study proposes using the complex frequency plane representation as a tool to quantify loss levels of a metamaterial at low sound levels, enabling the prediction of trends in absorption coefficient changes at high sound levels. A multi-resonant metamaterial composed of a series of thin annular cavities connected by a central perforation is considered which has been previously studied in the linear regime. With the analytical model developed for the linear regime, the representation of the complex frequency plane allows understanding whether a low value of absorption peak is due to excessive losses or, instead, to a lack of losses in the material. As sound level increase, material losses rise, leading to decrease in absorption peaks for structures with excessive losses and increase of peak absorption coefficient values for those with insufficient losses. Multi-resonant metamaterials with a constant main pore profile are selected to exhibit resonances with various loss levels, and measurements in a high sound level impedance tube are conducted to validate the expected changes in absorption coefficient. After that, an acoustic black hole is considered and a structure with two low frequency absorption peaks increasing with sound level and presenting a broad absorption band with low sensitivity to high sound levels is identified. The predictions are validated experimentally.

1. Introduction

Development of effective sound absorbers is critical in extreme environments such as industrial settings. However, conventional materials often struggle to absorb sound effectively, especially at low frequencies, primarily due to the bulky nature of these materials and the need to limit their thickness in most applications. Additionally, their flammability renders them unsuitable for demanding environments. In contrast, acoustic metamaterials offer a promising solution in sound wave control, often with subwavelength thickness, and they can be made from non-inflammable materials. For acoustic absorption, these structured materials often consist of a periodic array of resonators [1,2], and more complex multi-resonant structures have also been investigated [3–5]. Dupont et al. [6] introduced a multi-resonant acoustic metamaterial composed of thin annular cavities connected by a central perforation. This material exhibits numerous absorption peaks, including those at low frequencies, which are below the quarter wavelength absorption peak of the perforation alone. Subsequent to [6], studies focused on some geometric variations for a lower frequency absorption peak [7,8]. Another study [9] investigated acoustic black hole (ABH) main pore profiles to achieve a broadband absorption. Profiles with a gradually decreasing main perforation were studied [10–12], and recently adapted to more complex structures [13,14]. In [9], the ABH profiles were tailored to a thin structure to achieve broadband absorption and the analyses of various profiles were conducted using complex frequency plane representation. This technique is particularly useful for visualizing resonance loss levels and their evolutions, as presented in [15]. It has been used in various structures such as sub-wavelength absorbers [16], pipe mufflers [17], or even earplugs [18]. Recently, the complex frequency plane representation has been utilized to the analysis of rectangular sonic black holes [19].

In many industrial environments, the noise level can be considerable. The acoustic behavior of structured materials can differ significantly at high sound levels compared to linear levels. Pioneering work [20,21] has shown that as the sound level increases, turbulence in the form of vortices is generated at the edges of orifices. Subsequently, the acoustic behavior of various structured materials has been studied under high sound levels, such as microperforated panels (MPP) [22 23,24],

* Corresponding author.
E-mail address: gauthier.bezancon.1@ens.etsmtl.ca (G. Bezançon).

https://doi.org/10.1016/j.apacoust.2025.110529
Received 21 June 2024; Received in revised form 19 November 2024; Accepted 2 January 2025
Available online 18 January 2025

Helmholtz resonators [25,26], or structures with more complex geometries [27–30]. To design materials considering these effects, many studies used an analytical model based on loss description, incorporating nonlinear resistance. For instance, the Forchheimer model, initially introduced for characterizing the nonlinear behavior of rigid porous materials [31–33], is also utilized for structured materials [23,28]. It considers a dependence of static flow resistivity on particle velocity in perforations, which varies with sound level. Therefore, an increase in sound level leads to increase of viscous losses within the structure. This can result in decreased absorption at high sound levels [27,28]. However, if the material does not achieve perfect absorption in the linear regime due to insufficient losses, then its absorption will increase in the non-linear regime [22,24,25,26,29]. Nevertheless, nonlinear models are mostly semi-empirical, requiring additional parameter measurements (or simulation), in each orifice for every sound level. This complexity makes them challenging to develop and to adapt to different structures. Nonetheless, assessing a material's loss level in the linear regime can provide quicker insights into its absorption behavior at high sound levels, aiding the determination of geometries with the desired absorption evolution.

In this study, it is proposed to use the complex frequency plane representation as a tool to quantify the loss level of a metamaterial, using a linear model. Together with simple analysis of the nonlinear effects, this enables the direct anticipation of absorption peak evolution as the sound level increases, thereby facilitating the design of materials with improve absorption at high sound levels. This tool is examined for the multi-resonant metamaterial from [9], using the linear model developed, with modifications to its geometry to control loss level in the linear regime. Firstly, experimental measurements of the absorption coefficient at various sound levels are conducted for the metamaterial with a perfect absorption peak at low frequencies to assess the effect of nonlinearity on absorption. These measurements are analyzed using the complex frequency plane representation. Consequently, metamaterials with low losses in the linear regime are proposed to achieve improved absorption at high sound levels. These finding are confirmed by additional experimental measurements.

The paper is organized as follows. **Section 2** describes the experimental setup and details the analytical approaches used for the analysis. Then, in **section 3.1**, the complex frequency plane tool is employed to analyze absorption measurements at high sound levels for a constant reference profile and gain a deeper insight into the non-linear effects. In **Section 3.2**, a constant profile with low-losses in the linear regime is determined using this tool, and its expected acoustic behavior as the sound level increases is compared with experimental measurements. Finally in **Section 3.3**, a complex frequency plane representation is employed to propose an ABH profile with insufficient losses in the linear regime and its improved absorption at high sound levels is confirmed through experimentation.

2. Material and methods

2.1. Material

The studied multi-resonant metamaterial (see Fig. 1), proposed in [9], features a cylindrical overall structure with a radius of $R_{samp} = 22.2$ mm and a total thickness of $L = 31$ mm. It is composed of $N = 15$ thin annular cavities, each with an external radius of $R_{cav} = 21$ mm and a thickness of $h_{cav} = 1$ mm. These cavities are connected to the main perforation and are separated by annular plates, periodically positioned, each with a thickness of $h_{mp} = 1$ mm. The material is finished with a final, non-perforated plate. In this study, both constant (see Fig. 1 a)) and ABH (see Fig. 1 b)) main pore profiles are considered. A constant main pore profile is defined by a single main perforation radius value, r_{mp}. An ABH main pore profile is characterized by $N = 15$ different r^i_{mp} values, decreasing with thickness, summarized as $r_{mp} = r^1_{mp}$ to r^{15}_{mp}. Note

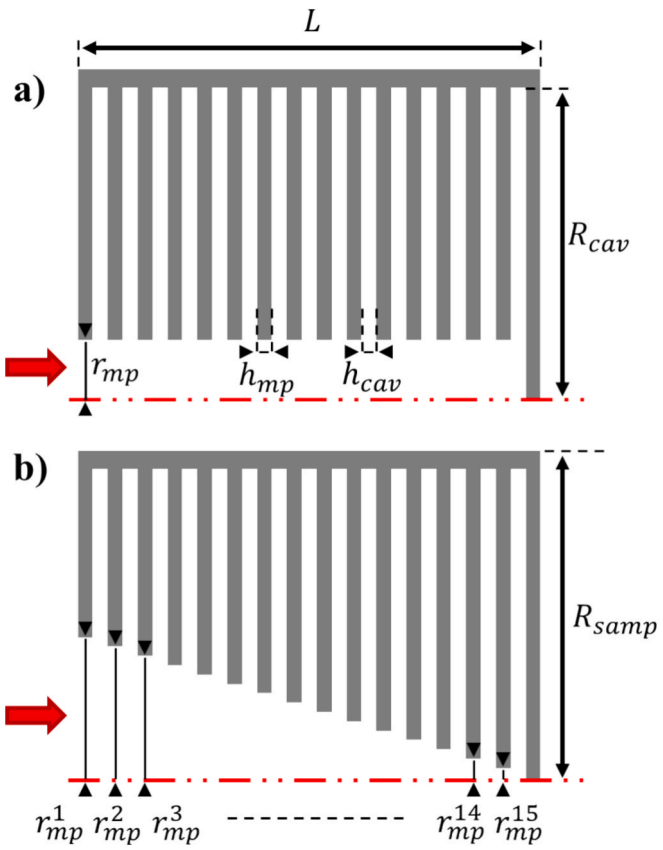

Fig. 1. 2D cross-sectional view of the studied metamaterial with a) constant and b) ABH main pore profile.

that this study is limited to linear ABH profiles. The main pore profile serves as the only variable geometric parameter used to control the level of losses in the material, while the other geometric parameters remain fixed.

The structure is constructed using an assembly of aluminum-machined cells. This ensures precision in the elements, particularly the circular shape of the main pores and the flat surfaces forming the thin cavities. Further details on the cells, assembly, and manufacturing process can be found in **Section 2.4** and Fig. 4 of [9].

2.2. Experimental set up

The experimental measurements are conducted using a high-sound-level impedance tube. The excitation consists of a sine sweep wave covering a frequency range from 300 Hz to 4 000 Hz. The sound level ranges from 100 dB to 145 dB. An adapter had to be designed and manufactured to transition from the source fixed on a 14.5 mm radius impedance tube to a 22.22 mm radius impedance tube, matching the structure under study. The length and slope of the homemade adapter were designed to ensure plane waves in the 22.22 mm radius tube section, where the microphones are placed. The absorption coefficient is calculated using the two-microphone method [34].

2.3. Analytical approach

This section outlines the linear analytical tools employed to characterize the acoustic behavior of the metamaterial in the linear regime. It covers the description of losses and introduces the complex frequency plane representation. Additionally, the aspects of nonlinearity are introduced to describe the evolution of absorption at high sound levels.

The linear model, developed in a previous study [9], employs a transfer matrix approach and represents thin cavities as lumped

elements. Each part of the structure corresponds to one or a group of elementary matrices of size 2 by 2. Thermo-viscous losses are taken into account by considering air in the main pore sections and in thin cavities as equivalent fluids, using parameters given by the Johnson-Champoux-Allard-Lafarge (JCAL) model. In this study, the focus is on viscous losses since only they change at high levels. Viscous losses are accounted for by the equivalent density. The expression for the equivalent density of air in each of the main pores i (i.e. in the circular perforations before each annular cavity) [35–37] is:

$$\tilde{\rho}^i = \frac{\alpha_\infty \rho_0}{\Phi}\left(1 + \frac{\sigma_0^i \Phi}{j\omega\alpha_\infty\rho_0}\sqrt{1 + \frac{4\alpha_\infty{}^2\eta\rho_0\omega}{\sigma_0^i{}^2\Lambda^i{}^2\Phi^2}}\right) \quad (1)$$

with ω the angular frequency, ρ_0 the density of the air, η the dynamic viscosity of the air, α_∞ the tortuosity, Φ the open porosity, Λ^i the viscous characteristic length and σ_0^i the static flow resistivity. The main pores are identified to circular cross-section pores with r_{mp}^i radius, thus $\alpha_\infty = 1$, $\Phi = 1$, $\Lambda^i = r_{mp}^i$ and the static flow resistivity is given by:

$$\sigma_0^i = 8\eta / r_{mp}^i{}^2\Phi \quad (2)$$

The product of all the elementary matrices yields the total sample matrix $\boldsymbol{T}_{samp}$. From the elements of $\boldsymbol{T}_{samp}$, the normal incidence reflection coefficient for a sample backed by a wall is given by:

$$R = \frac{T_{samp,11} - T_{samp,21}Z_0}{T_{samp,11} + T_{samp,21}Z_0} \quad (3)$$

with Z_0 the characteristic impedance of the air and therefore, the normal incidence absorption coefficient is $\alpha = 1 - |R|^2$. The complex frequency representation involves plotting the value of $20\log_{10}(R)$ on a plane with real (x-axis) and complex (y-axis) frequencies. Material resonances are depicted by pairs of a pole (local maximum) and a zero (local minimum) positioned at the same real frequency [15]. The position of a zero on y-axis indicates the loss level of the corresponding resonance and thus an indication of the amplitude of the corresponding absorption peak: if the zero is positioned below the real frequency axis (see Fig. 2 a)), the absorption peak value is less than 1 due to excessive losses (see Fig. 2 b)); if it is on the axis (see Fig. 2 c)), the absorption peak is a perfect absorption peak (see Fig. 2 d)); and if it is above (see Fig. 2 e)), the absorption peak value is less than 1 due to insufficient losses (see Fig. 2 f)). Moreover, a broader colored spot around a zero (see Fig. 2 g)), which is also linked to a greater distance between the pole and the zero, corresponds to a broader absorption peak (see Fig. 2 h)).

At high sound levels, the material exhibits nonlinear effects. One approach to consider these effects is to introduce nonlinearity by establishing a dependence between the flow resistivity σ^i and flow rates $V_f{}^i$ in a pore through the Forchheimer's law [28]:

$$\sigma^i(V_f) = \sigma_0^i(1 + \xi^i V_f{}^i) \quad (4)$$

with ξ^i Forchheimer's non linearity parameter that can be determined by measurements or FEM simulations. In acoustic models, the flow rate is replaced with the maximum particle velocity amplitude, see e.g. [28]. As the sound level increases, the maximum particle velocity amplitudes in the main pores also increase, leading to higher flow resistivities σ^i. By revisiting **Eq. (1)** and replacing the static flow resistivity σ_0^i with the flow resistivity σ^i, it can be observed that if σ^i increases, the imaginary part of the equivalent density of the main pores $\tilde{\rho}^i$ also increases. Thus, an increase in sound level results in an increase in losses in the main pores. Note that the thin annular cavities do not affect the equivalent density and only modify the effective bulk modulus, which remains linear at high sound levels [28]. Here, only the static flow resistivity is modified through the Forchheimer parameter. This allows for predicting how the material's loss level changes as the sound level increases, thereby foreseeing the evolution of absorption.

3. Results

3.1. Constant reference profile with $r_{mp} = 2$ mm

In this section, the acoustic behavior at high sound levels of the first metamaterial characterized by a constant main pore radius $r_{mp} = 2$ mm is investigated. It has been previously studied in the linear regime [6,9], and it is known to exhibit a high first absorption peak at low frequencies, close to perfect absorption.

The measured absorption coefficient of this material for sound levels ranging from 100 dB to 145 dB is presented in Fig. 3 a). Throughout this

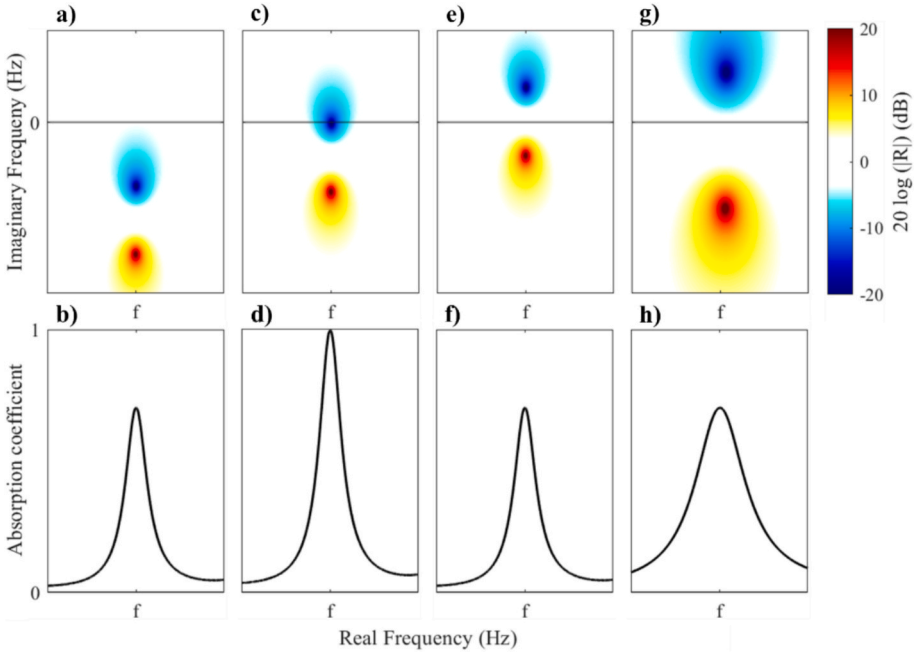

Fig. 2. Examples of resonance visualization using the complex frequency plane representation.

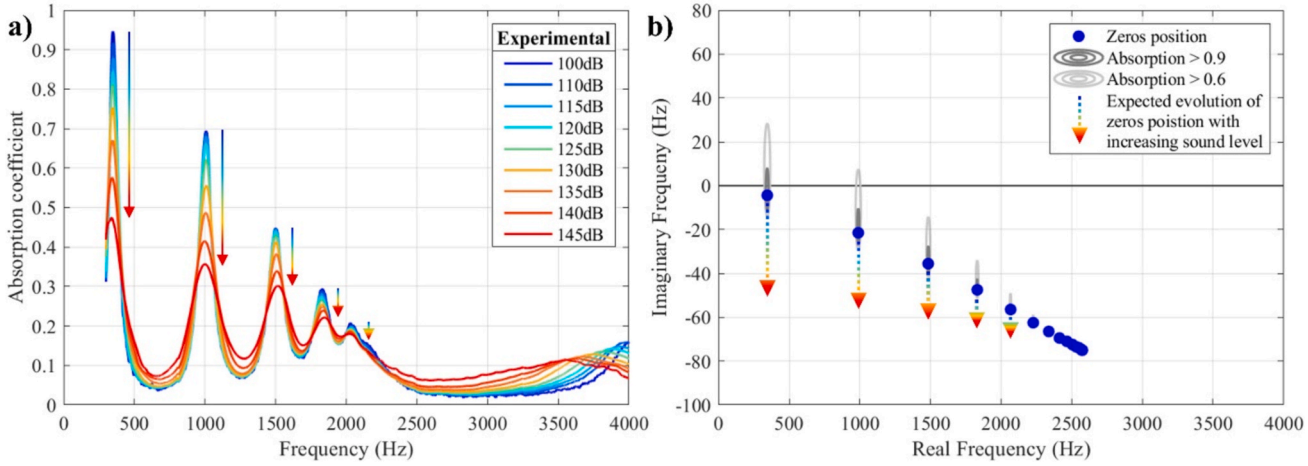

Fig. 3. Metamaterial with a constant main pore profile $r_{mp} = 2$ mm: a) experimental absorption coefficient as a function of sound level and b) position of zeros in the representation of the complex frequency plane of the reflection coefficient from the linear analytical model and the expected evolution of the first zeros position with increasing sound level.

study, the sound level of 100 dB is considered to be in the linear regime, indicated in dark blue, while above 110 dB is considered to be in the nonlinear regime, ranging from light blue to red for 145 dB. In the linear regime (in dark blue), the absorption curve exhibits five peaks between 300 Hz and 2100 Hz and the beginning of a band gap around 2500 Hz. As the sound level increases, the frequency positions of all absorption peaks remain almost unchanged, but their amplitudes decrease significantly. It is noteworthy that the decrease is particularly significant for peaks at lower frequencies which are mostly controlled by the losses in the main pores: −50 % for the first peak, −48 % for the second, −31 % for the third, −24 % for the fourth, and −12 % for the fifth. Conversely, the values of the troughs between the absorption peaks increase slightly with the sound level.

The reflection coefficient from the analytical model (**Eq. (3)**) of the material under linear regime is plotted in the complex frequency plane in Fig. 3 b). For clarity, only the zeros, i.e., local minima, and two "*iso*-absorption zones," which correspond to the regions around a zero with a corresponding absorption value greater than 0.6 or 0.9, are indicated in this figure. There are 15 zeros corresponding to 15 resonances, matching the number of thin cavities. The first 5 zeros correspond to the 5 identified absorption peaks. The first zero, at 350 Hz, is close to the real frequency axis, which is consistent with known results and the proximity of the first experimental peak to perfect absorption in the linear regime (see Fig. 3 a)). Subsequent zeros progressively deviate from the real frequency axis, corresponding to the lower absorption peak values. All zeros are positioned below the real frequency axis, indicating that the material exhibits resonances with excessive losses in the linear regime.

As is shown in **section 2.3**, with increasing sound levels, the flow resistivities σ^i of the main pore segments increase, thus, leading to higher losses. In the complex frequency plane, this increase in losses results in a downward shift of the zeros toward the y-axis. Additionally, it has been experimentally observed (in Fig. 3 a)) that absorption peaks at lower frequencies are more sensitive to high sound levels. Consequently, dotted arrows have been added to Fig. 3 b) to indicate the expected corresponding displacement of the zeros as the sound level increases, consistent with these observations and insights gained. These downward shifts of the zeros in the complex frequency plane correspond to decrease in absorption coefficient peak values, as shown in the experimental results in Fig. 3 a).

Therefore, assessing the amount of losses in the linear regime using the complex frequency plane has provided valuable insights into the evolution of absorption peaks at high sound levels. For this multi-resonant metamaterial profile, absorption peaks decrease significantly as the sound level increases because resonances already have excessive losses in the linear regime. The following section aims to analyze the absorption at high sound levels of another constant main pore profile material, featuring resonances with lower losses in the linear regime.

3.2. *Constant profile with* $r_{mp} = 4$ *mm*

In this section, a constant main pore profile with low losses in the linear regime is determined, and its acoustic behavior at high sound levels is analyzed. In the linear regime, increasing the main pore radius decreases the static flow resistivity $\sigma_0{}^i$ (see **Eq. (2)**). This reduces the imaginary part of the equivalent density within the main pore (see **Eq. (1)**), leading to a decrease in losses. Also, modifying the main pore radius alters the metamaterial's geometry, which influences the resonance frequencies and hence the absorption peaks' positions [9]. With a constant profile, the loss levels among resonances are unbalanced, although the initial resonances can exhibit significantly lower losses with a large enough main pore radius. The profile investigated in this section is the constant main pore radius of $r_{mp} = 4$ mm, chosen to exhibit the first resonance with low losses, a second one close to perfect absorption, and subsequent resonances with excessive losses, in the linear regime.

The positions of its zeros on the complex frequency plane, for the linear regime, are shown in Fig. 4 a). The first zero is positioned above the real frequency axis, indicating insufficient losses. The second zero is close to the horizontal axis, corresponding to a resonance with perfectly balanced losses. The subsequent zeros are positioned below this axis, indicating resonances with excessive losses. It is worth noting that the *iso*-absorption zones around the zeros are wider and larger than those of the constant profile with $r_{mp} = 2$ mm. Wider zones around a zero along the x-axis corresponds to broader absorption peak. Furthermore, as the sound level increases, it is expected that the zeros shift downward relative to the y-axis, as discussed in previous sections. This downward shift is anticipated to be more pronounced at lower frequencies compared to higher ones, as observed for the profile considered earlier. Consequently, it is expected that the value of the first absorption coefficient peak increases with sound level. The values of the subsequent peaks should decrease, as their corresponding zeros move further away from the real frequency axis in complex plane.

The measured absorption coefficient for different sound levels is depicted in Fig. 4 b). In the linear regime, the absorption curve (in dark blue) exhibits four absorption peaks: the first at 670 Hz has a maximum peak value of 0.84, the second one at 1790 Hz is close to perfect absorption with 0.96, the third at 2403 Hz is at 0.65, and the fourth at 2740 Hz is at 0.35. These experimental results in the linear regime align

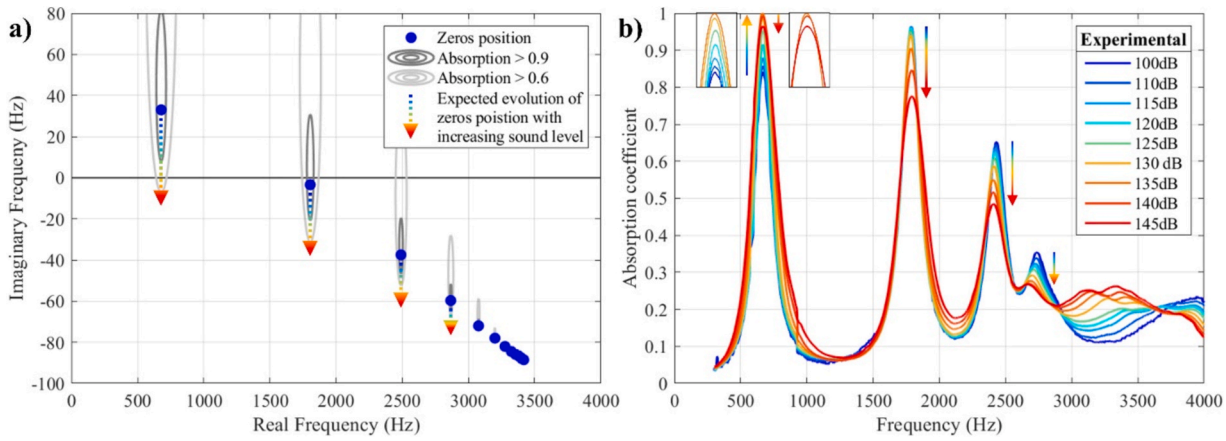

Fig. 4. Metamaterial with a constant main pore profile $r_{mp} = 4$ mm: a) position of zeros in the representation of the complex frequency plane of the reflection coefficient from the linear analytical model and the expected evolution of the first zeros with increasing sound level, and b) experimental absorption coefficient as a function of sound level.

well with the position of zeros and *iso*-absorption lines shown in Fig. 4 a). As the sound level increases, the frequency positions of the absorption peaks change verry little, but their values change significantly. The first absorption peak increases until perfect absorption is reached at 130 dB and then decreases slightly. The following three peaks decrease with increasing sound level. These trends align with the expected behavior of the zero positions. Indeed, for the first resonance, which has low losses, the zero is located above the real frequency axis. As the sound level increases, its position on a complex frequency plane shifts toward the real frequency axis and then moves away from it. This corresponds to an absorption peak that increases to perfect absorption and then decreases. This behavior has been observed for an MPP backed by an air cavity by Tayong et al. [22]. For the subsequent resonances, which are already with excessive losses, as the sound level increases and the losses increase too, the zeros shift downward and move away from the real frequency axis, resulting in a decrease in the absorption peaks.

Furthermore, it can be observed that the proportional variation of absorption with increasing sound level is less significant compared to the profile from the previous section. The first peak increases by 19 % then decreases by −5%, the second decreases by −19 %, and the third peak decreases by −26 %. This could be attributed to the slower increase in the particle velocity as the sound level increases because the main pore is larger. Thus, the flow resistivity σ increases less with the sound level (see **Eq. (4)**), resulting in less pronounced losses and consequently, less variation in absorption peaks. Additionally, for this profile, the absorption peaks vary less for the first two peaks than for the third, unlike the $r_{mp} = 2$ mm profile. This may be explained by the fact that the *iso*-absorption zones are larger along the y-axis for this profile. Indeed, when the sound level increases and a zero is near the real frequency axis, the value remains high longer if the spot is larger. This results in a smaller variation in the absorption peak value within this range. This is notably observable for the 2nd absorption peak, which exhibits minimal variation between 100 dB and 130 dB (−2%), but considerably more between 130 and 145 dB (−17 %).

Therefore, a constant profile with a larger main pore allows resonances with low losses in the linear regime, resulting in absorption peaks that can increase in value with the sound level. Additionally, this enables peaks to be less sensitive to high levels and to remain close to perfect absorption over a wider range of sound levels. However, with a constant profile, some absorption peaks remain low due to an uneven distribution of losses among the resonances. The next section aims to investigate the acoustic behavior at high sound levels of an ABH profile, which exhibits resonances with less disparity in losses in the linear regime [9].

3.3. ABH profile with $r_{mp} = 9$ mm to 2 mm

In this section, an ABH main pore profile is determined to achieve broadband absorption at high sound levels. The aim is to identify a profile exhibiting resonances with low losses in the linear regime, and high absorption peaks at high sound levels, with subsequent peaks closely spaced in frequency, relatively high, and less sensitive to further increase in sound level. ABH profiles have been extensively studied in the linear regime [9]. A large perforation radius at the front of the profile, r^1_{mp}, reduces the loss levels of all resonances, resulting in higher absorption peaks at high frequency. The radius of the main pore at the back of the profile, r^{15}_{mp}, primarily affects the loss levels of low-frequency resonances, aiming to balance losses across resonances. The profile investigated in this section is the ABH profile with $r_{mp} = 9$ mm to 2 mm, shown in Fig. 1 b). It has been selected to exhibit two low losses resonances, followed by subsequent resonances that are closely spaced in frequency. Its characteristics in the linear regime are presented first, followed by an analysis of its acoustic behavior at high sound levels.

Fig. 5 a) depicts the zero positions of this material on the complex frequency plane with two *iso*-absorption lines. The first two zeros are located above the real frequency axis, corresponding to resonance with low losses in the linear regime. The subsequent zeros are positioned below the real frequency axis, representing resonances with excessive losses, which are spaced relatively close to each other. Furthermore, they exhibit more extensive *iso*-absorption zones than the previously studied profiles. As shown in [9] (see **Section 3.3**), at high frequencies, the acoustic behavior of the material is determined only by its front, where thin annular cavities have not yet reached their local resonance. Thus, it becomes equivalent to a truncated and therefore shorter material with a larger main pore. As seen in the two previous sections, a larger main pore in this metamaterial leads to wider and larger *iso*-absorption zones around zeros. In this profile, this results in wider absorption peaks at high frequency, contributing to a broad absorption coefficient band. Based on the conclusions drawn in earlier sections, the zeros should shift downward as the sound level increases. As a result, the first two zeros should move closer to the real frequency axis, leading to an increase in the values of the first two absorption peaks. For the subsequent peaks, since their corresponding zeros are already positioned below the real frequency axis in the linear regime, the absorption peaks should decrease, due to the presence of significantly larger *iso*-absorption zones, though less sharply than in the previous profiles.

The experimentally measured absorption coefficient of this material for various sound levels is plotted in Fig. 5 b). In the linear regime, the curve (in dark blue) exhibits two absorption peaks at medium frequency: one at 1020 Hz with an amplitude of 0.75 and another at 1904 Hz with

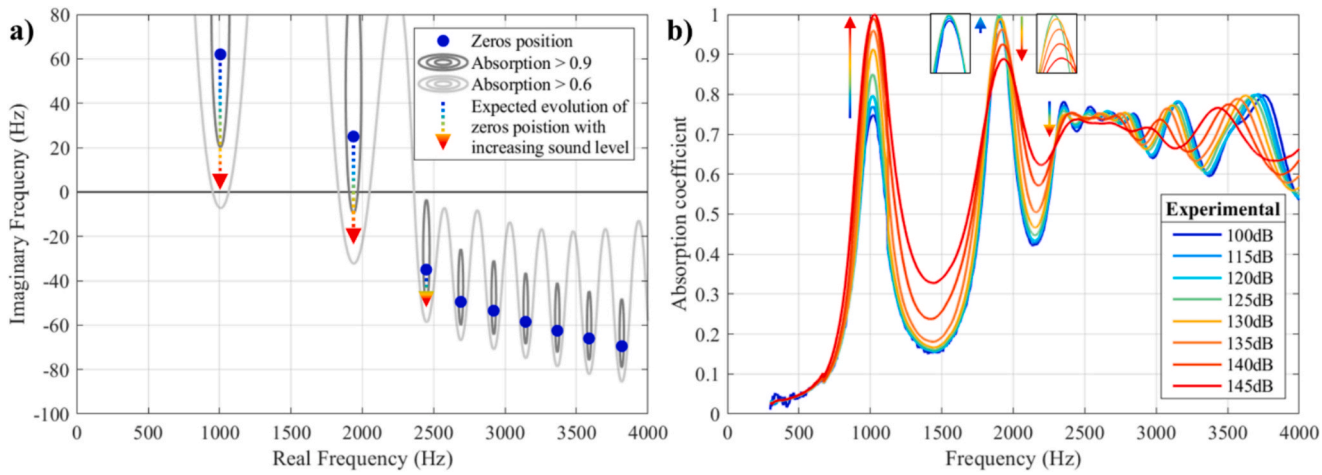

Fig. 5. Metamaterial with a linear ABH profile $r_{mp} = 9$ to 2 mm: a) position of zeros in the representation of the complex frequency plane of the reflection coefficient from the linear analytical model and the expected evolution of the first zeros with increasing sound level, and b) experimental absorption coefficient as a function of sound level.

an amplitude of 0.98. Then, there is a broad absorption band composed of multiple peaks starting from 2300 Hz and above 0.6 in amplitude. These observations in the linear regime align well with the *iso*-absorption zones along the real frequency axis in Fig. 5 a). As the sound level increases, the first peak increases until it reaches perfect absorption at 145 dB. The second peak also increases, achieving perfect absorption at 125 dB, and then decreases to 0.89 absorption at 145 dB. Similar to the second absorption peak in the profile of the previous section, this peak changes minimally between 100 dB and 130 dB because the corresponding zero is close to the real frequency axis and the *iso*-absorption zones are relatively large. The subsequent peaks, forming the absorption band, decrease very slightly and remain above 0.6 absorption. This corresponds well to the expected evolution of the zeros position on the complex frequency plane as the sound level increases.

Therefore, the absorption of this ABH structure improves as the sound level increases. At 145 dB, the material exhibits a perfect absorption peak at 1020 Hz, along with a broad band from 1750 Hz to 4000 Hz with absorption exceeding 0.62. Furthermore, without a comprehensive analytical model for high sound levels, the main features of this material performance in the nonlinear regime could be directly predicted using complex frequency plane analysis.

4. Conclusion

This study aims to use the complex frequency plane analysis as a tool to analyze absorption performance of structured acoustical materials under high sound levels. This technique allows to quantify the loss level of resonances in the linear regime. Based on the knowledge that flow resistivity is the parameter mostly affected by nonlinear effects, the complex frequency plane analysis enables quick prediction of absorption peak evolution with increase of the sound level. This approach is useful for design of metamaterials with enhanced absorption under high sound levels. In this study, it was applied to a thin multi-resonant metamaterial. The ABH profile is identified with the help of complex plane analysis which demonstrates enhanced broadband absorption under high excitation levels. This effect is observed in experiments and showcases the material's potential for absorption in extreme environments. However, precisely predicting the magnitude of shift of zeros under high levels in the complex frequency plane and their optimal placement in the linear regime with this approach is challenging without a true nonlinear model. Nevertheless, this tool can complement analytical and numerical models at high sound levels, aiding in the rapid identification of promising geometries.

Funding sources

The authors acknowledge the financial support of Natural Sciences and Engineering Research 545 Council (NSERC) [funding reference numbers: RGPIN-2019-06573].

Declaration of Generative AI and AI-assisted technologies in the writing process

During the preparation of this work the authors used ChatGPT in order to improve the readability and language of the manuscript. After using this tool, the authors reviewed and edited the content as needed and take full responsibility for the content of the publication.

CRediT authorship contribution statement

Gauthier Bezançon: Writing – original draft, Visualization, Methodology, Formal analysis, Conceptualization. **Olivier Doutres:** Writing – original draft, Supervision, Methodology, Conceptualization. **Olga Umnova:** Writing – review & editing, Methodology. **Philippe Leclaire:** Writing – review & editing. **Thomas Dupont:** Writing – original draft, Supervision, Methodology, Conceptualization.

Declaration of competing interest

The authors declare that they have no known competing financial interests or personal relationships that could have appeared to influence the work reported in this paper.

Data availability

Data will be made available on request.

References

[1] Leclaire P, Umnova O, Dupont T, Panneton R. Acoustical properties of air-saturated porous material with periodically distributed dead-end pores. J Acoust Soc Am 2015;137(4):1772–82. https://doi.org/10.1121/1.4916712.
[2] Jiménez N, Romero-García V, Pagneux V, Groby J. Quasiperfect absorption by subwavelength acoustic panels in transmission using accumulation of resonances due to slow sound. Phys Rev B 2017;95(1). https://doi.org/10.1103/physrevb.95.014205.
[3] Yang X, Shen X, Yang F, Yin Z, Yang F, Yang Q, et al. Acoustic metamaterials of modular nested Helmholtz resonators with multiple tunable absorption peaks. Appl Acoust 2023;213:109647. https://doi.org/10.1016/j.apacoust.2023.109647.
[4] Liu Q, Yang J, Tang Y, Li H, Xu Y, Liu X, et al. A multi-layered corrugated resonator acoustic metamaterial with excellent low-frequency broadband sound absorption

performance. Appl Acoust 2024;216:109800. https://doi.org/10.1016/j.apacoust.2023.109800.
[5] Marescotti C, Pompoli F. Geometric optimisation of a multiple coiled-up resonator for broadband and octave band acoustic absorption. Appl Acoust 2024;221:110000. https://doi.org/10.1016/j.apacoust.2024.110000.
[6] Dupont T, Leclaire P, Panneton R, Umnova O. A microstructure material design for low frequency sound absorption. Appl Acoust 2018;136:86–93. https://doi.org/10.1016/j.apacoust.2018.02.016.
[7] Kone TC, Lopez M, Ghinet S, Dupont T, Panneton R. Thermoviscous-acoustic metamaterials to damp acoustic modes in complex shape geometries at low frequencies. J Acoust Soc Am 2021;150(3):2272–81. https://doi.org/10.1121/10.0006441.
[8] Lopez M, Dupont T, Panneton R. Mass-spring model for acoustic metamaterials consisting of a compact linear periodic array of dead-end resonators. J Acoust Soc Am 2024;155(1):530–43. https://doi.org/10.1121/10.0024212.
[9] Bezançon G, Doutres O, Umnova O, Leclaire P, Dupont T. Thin metamaterial using acoustic black hole profiles for broadband sound absorption. Appl Acoust 2024;216:109744. https://doi.org/10.1016/j.apacoust.2023.109744.
[10] Ouahabi, A. A. E., Krylov, V. V., & O'Boy, D. (2015). Experimental investigation of the acoustic black hole for sound absorption in air. The 22nd International Congress on Sound and Vibration, 2015. Florence, Italy.
[11] Guasch O, Arnela M, Sánchez-Martín P. Transfer matrices to characterize linear and quadratic acoustic black holes in duct terminations. J Sound Vibrat 2017;395:65–79. https://doi.org/10.1016/j.jsv.2017.02.007.
[12] Umnova O, Brooke D, Leclaire P, Dupont T. Multiple resonances in lossy acoustic black holes - theory and experiment. J Sound Vibrat 2023;543:117377. https://doi.org/10.1016/j.jsv.2022.117377.
[13] Chen Y, Yu K, Fu Q, Zhang J, Lu X, Du X, et al. A broadband and low-frequency sound absorber of sonic black holes with multi-layered micro-perforated panels. Appl Acoust 2024;217:109817. https://doi.org/10.1016/j.apacoust.2023.109817.
[14] Peng L, Mao Q, Wang H, Lai L, Shi Q, Chen L. Enhanced sound absorption with the combined sonic black holes. Appl Acoust 2024;219:109932. https://doi.org/10.1016/j.apacoust.2024.109932.
[15] Romero-García V, Theocharis G, Richoux O, Pagneux V. Use of complex frequency plane to design broadband and sub-wavelength absorbers. J Acoust Soc Am 2016;139(6):3395–403. https://doi.org/10.1121/1.4950708.
[16] Jiménez N, Romero-García V, Pagneux V, Groby J. Rainbow-trapping absorbers : Broadband, perfect and asymmetric sound absorption by subwavelength panels for transmission problems. Sci Rep 2017;7(1). https://doi.org/10.1038/s41598-017-13706-4.
[17] Zhang D, Su X, Liu Y, Luo Y, Sun X, Chen C. Performance study and improvement of space-folded metamaterial muffler for pipe under grazing flow. Appl Acoust 2024;220:109984. https://doi.org/10.1016/j.apacoust.2024.109984.
[18] Carillo K, Sgard F, Dazel O, Doutres O. Reduction of the occlusion effect induced by earplugs using quasi perfect broadband absorption. Scient Rep (Nat Publish Group) 2022;12(1). https://doi.org/10.1038/s41598-022-19641-3.
[19] Hruška V, Groby J, BednaříK M. Complex frequency analysis and source of losses in rectangular sonic black holes. J Sound Vibrat 2024;571:118107. https://doi.org/10.1016/j.jsv.2023.118107.
[20] Ingård U, Labate S. Acoustic circulation effects and the nonlinear impedance of orifices. J Acoust Soc Am/J Acoust Soc Am 1950;22(2):211–8. https://doi.org/10.1121/1.1906591.
[21] Ingård U, Ising H. Acoustic nonlinearity of an orifice. J Acoust Soc Am 1967;42(1):6–17. https://doi.org/10.1121/1.1910576.
[22] Tayong R, Dupont T, Leclaire P. On the variations of acoustic absorption peak with particle velocity in micro-perforated panels at high level of excitation. J Acoust Soc Am 2010;127(5):2875–82. https://doi.org/10.1121/1.3372714.
[23] Tayong R, Dupont T, Leclaire P. Experimental investigation of holes interaction effect on the sound absorption coefficient of micro-perforated panels under high and medium sound levels. Appl Acoust 2011;72(10):777–84. https://doi.org/10.1016/j.apacoust.2011.04.011.
[24] Laly Z, Atalla N, Meslioui S. Acoustical modeling of micro-perforated panel at high sound pressure levels using equivalent fluid approach. J Sound Vibrat 2018;427:134–58. https://doi.org/10.1016/j.jsv.2017.09.011.
[25] Achilleos V, Richoux O, Theocharis G. Coherent perfect absorption induced by the nonlinearity of a Helmholtz resonator. J Acoust Soc Am 2016;140(1):EL94-EL100. https://doi.org/10.1121/1.4954869.
[26] Zhu J, Qu Y, Gao H, Meng G. Nonlinear sound absorption of Helmholtz resonators with serrated necks under high-amplitude sound wave excitation. J Sound Vibrat 2022;537:117197. https://doi.org/10.1016/j.jsv.2022.117197.
[27] Tang Y, He W, Xin F, Lu TJ. Nonlinear sound absorption of ultralight hybrid-cored sandwich panels. Mechan Syst Signal Process 2020;135:106428. https://doi.org/10.1016/j.ymssp.2019.106428.
[28] Brooke D, Umnova O, Leclaire P, Dupont T. Acoustic metamaterial for low frequency sound absorption in linear and nonlinear regimes. J Sound Vibrat 2020;485:115585. https://doi.org/10.1016/j.jsv.2020.115585.
[29] Zhu J, Gao H, Dai S, Qu Y, Meng G. Multilayer structures for high-intensity sound energy absorption in low-frequency range. Int J Mech Sci 2023;247:108197. https://doi.org/10.1016/j.ijmecsci.2023.108197.
[30] Sun W, Chu Z, Lang Y. Nonlinear sound absorption of coiling-up space under high amplitude acoustic excitation. Appl Acoust 2024;220:109956. https://doi.org/10.1016/j.apacoust.2024.109956.
[31] Wilson DK, McIntosh JD, Lambert RF. Forchheimer-type nonlinearities for high-intensity propagation of pure tones in air-saturated porous media. J Acoust Soc Am 1988;84(1):350–9. https://doi.org/10.1121/1.396937.
[32] Aurégan Y, Pachebat M. Measurement of the nonlinear behavior of acoustical rigid porous materials. Phys Fluids 1999;11(6):1342–5. https://doi.org/10.1063/1.869999.
[33] Umnova O, Attenborough K, Standley E, Cummings A. Behavior of rigid-porous layers at high levels of continuous acoustic excitation: theory and experiment. J Acoust Soc Am 2003;114(3):1346–56. https://doi.org/10.1121/1.1603236.
[34] ISO 10534-2:2023, Acoustics – Determination of acoustic properties in impedance tubes Part 2: Two-microphone technique for normal sound absorption coefficient and normal surface impedance. Geneva, Switzerland: International Organization for Standardization; 2023.
[35] Johnson DL, Koplik J, Dashen R. Theory of dynamic permeability and tortuosity in fluid-saturated porous media. J Fluid Mech 1987;176(1):379. https://doi.org/10.1017/s0022112087000727.
[36] Champoux Y, Allard JF. Dynamic tortuosity and bulk modulus in air-saturated porous media. J Appl Phys 1991;70(4):1975–9. https://doi.org/10.1063/1.349482.
[37] Lafarge D, Lemarinier P, Allard JF, Tarnow V. Dynamic compressibility of air in porous structures at audible frequencies. J Acoust Soc Am 1997;102(4):1995–2006. https://doi.org/10.1121/1.419690.